

Surface acoustic wave propagation in monolayer graphene

Peter Thalmeier,¹ Balázs Dóra,^{2,*} and Klaus Ziegler³

¹Max-Planck-Institut für Chemische Physik fester Stoffe, 01187 Dresden, Germany

²Max-Planck-Institut für Physik komplexer Systeme, Nöthnitzer Str. 38, 01187 Dresden, Germany

³Institut für Physik, Universität Augsburg, D-86135 Augsburg, Germany

(Dated: October 29, 2018)

Surface acoustic wave (SAW) propagation is a powerful method to investigate 2D electron systems. We show how SAW observables are influenced by coupling to the 2D massless Dirac electrons of graphene and argue that Landau oscillations can be observed as function of gate voltage for constant field. Contrary to other transport measurements, the zero-field SAW propagation gives the wave vector dependence of graphene conductivity for small wave numbers. We predict a crossover from Schrödinger to Dirac like behaviour as a function of gate voltage, with no attenuation in the latter for clean samples.

PACS numbers: 43.35.Cg,81.05.Uw,73.20.-r

Sound waves in solids may be used as diagnostic tool to investigate the low frequency long wavelength response of electrons. In metals they couple via the deformation potential mechanism, i.e. stress dependence of kinetic energy. In semiconductors the piezoelectric mechanism which generates internal electric fields that accelerate the charge carriers is most effective provided the compound has a piezoelectrically active structure. Close to smooth surfaces the acoustic modes may become localized in the direction of the surface normal and propagate as surface acoustic waves (SAW). The most prominent ones are Rayleigh waves [1] where the displacement vector $\mathbf{u}(t)$ lies in the 'sagittal plane' formed by the surface normal vector $\hat{\mathbf{n}}$ and the acoustic propagation vector \mathbf{q} which is parallel to the surface (normal to $\hat{\mathbf{n}} \equiv \hat{\mathbf{z}}$, cf. Fig. 1). The Rayleigh SAW may be thought as consisting of longitudinal and transverse components whose amplitudes depend on the normal direction in a manner that the surface fulfills the mechanical stress free boundary condition. The Rayleigh wave is therefore an elliptically polarized wave in the sagittal plane which decays exponentially into the bulk with an acoustic penetration depth that is of the order of the bulk wavelength.

Because of these properties the Rayleigh SAW exhibit interesting effects due to the coupling to charge carriers, particularly in the presence of a magnetic field. Two of those are well known and have been explored experimentally. i) when the field is within the surface plane and perpendicular to the sagittal (xz) plane then due to the breaking of time reversal invariance the velocity of propagation of SAW with wave vectors \mathbf{q} and $-\mathbf{q}$ is different. This non-reciprocal SAW effect has been investigated for metals in detail in Ref. 2, 3. ii) In semiconductor heterostructures the charge carriers are confined in the lateral (xy) plane and a 2D electron gas (2DEG) forms. This may be nicely investigated by Rayleigh SAW which are localized on the surface sheet. For fields perpendicular to the surface they probe the longitudinal wave vector dependent conductivity of the 2DEG. Since the latter

exhibits the typical Landau quantum oscillations under suitable conditions this may be directly seen in the SAW propagation velocity and attenuation as function of magnetic field. This idea was spectacularly confirmed for the 2 DEG in GaAs heterojunctions [4, 5]. Extended investigations have shown that this method also allows uniquely to determine the wave-vector dependence of longitudinal conductivity [6].

The 2DEG in GaAs heterostructure contains electrons with non-relativistic parabolic dispersion and hence a finite band mass. Recently graphene, a single sheet honeycomb carbon layer, has been identified as a genuine 2DEG system[7]. It contains quasi-relativistic massless Dirac electrons with a linear dispersion around the Dirac point K where the slope is given by the Fermi velocity $v_F = 10^6$ m/s, obeying to

$$H = v_F(\sigma_x p_x + \sigma_y p_y), \quad (1)$$

where the pseudospin variables (σ) arise from the two-sublattice structure. The transport and thermodynamic properties of this system has been much discussed and investigated, in particular in an external field [8, 9]. They are distinctly different from the non-relativistic case which is mostly due to two effects: i) because of the linear dispersion the density of states (DOS) at the Dirac point $E = 0$ vanishes according to $N(E) = |E|/D^2$ (per valley and spin; $D^2 = 2\pi v_F^2/A_c$, where A_c is the area of the hexagonal cell). As a consequence the screening properties of Dirac electrons will be different from those of the nonrelativistic case [10, 11]. ii) The Landau quantization in an external magnetic field leads to relativistic Landau levels at $E_\alpha(n) = \alpha\omega_c\sqrt{n+1}$ with $\alpha = \pm 1$, $n = 0, 1, 2, \dots$ and the Landau scale $\omega_c = v_F\sqrt{2e|B|}$. In addition there is a field independent level always at $E^* = 0$.

There has been considerable discussion whether the Dirac point and the linear DOS in single layer graphene is stable against perturbations like buckling, disorder or excitonic gap formation. We ignore these subtle issues here and refer to the literature [9]. Furthermore we note

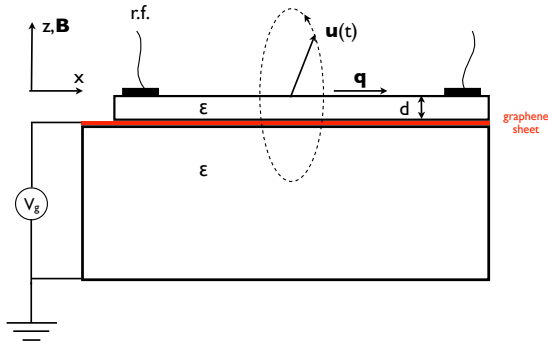


FIG. 1: Schematic setup for SAW propagation on monolayer graphene sandwiched between piezoelectric slabs with dielectric constant ϵ as adapted from Ref. 12. SAW transducer and detector are attached to the top slab with thickness $qd \ll 1$ ($q = \text{SAW wave number}$). The SAW displacement $\mathbf{u}(t)$ at fixed position traces an ellipse in the sagittal (xz) plane and the penetration depth in $-z$ direction is $\sim 2\pi/q \gg d$. Direction of field \mathbf{B} is normal to the surface.

that the chemical potential μ may be easily moved away from the Dirac point by applying a gate voltage V_g via $V_g \sim n \sim \mu^2$ [13] (with n the carrier density). This is a new aspect as compared to the degenerate nonrelativistic 2DEG and we will employ it in our discussion of SAW propagation effects in graphene. Preliminary SAW experiments in zero field have been performed in Ref. 14. In this setup the aim was rather to detect surface adsorbates via their change of graphene electronic properties and ensuing SAW propagation anomalies. In the present work we want to look at intrinsic properties of graphene and investigate the field dependence, gate voltage (chemical potential) and wave vector dependence of the SAW propagation velocity and attenuation. A possible experimental setup which we have in mind is shown schematically in Fig. 1. The graphene sheet is sandwiched between two insulating piezoelectric layers with the same background dielectric constant ϵ , similarly to Ref. 15. The SAW r.f. transducer and the detector are mounted on the top layer. Its thickness d is assumed to be much smaller than the penetration depth of the SAW along $-z$. There may also be alternatives where the coupling of SAW in the piezoelectric substrate to the Dirac electrons happens purely capacitive across an empty space.

The analysis of SAW propagation in this setup has two distinct steps. Firstly the mechanical and electrodynamic boundary value problem for the SAW has to be solved which gives the SAW velocity change in terms of the (magneto-) conductive properties of the graphene sheet. This problem has been analyzed and solved in Ref. 12. In a second step we calculate the magnetoconductivity of Dirac electrons as function of field and chem-

ical potential which leads to the SAW velocity change and attenuation as function of field and gate voltage. In this part we follow the procedure described in Ref. 16. Alternatively we consider the zero field case and investigate the wave vector (or frequency) dependence of SAW properties, which is related to the wave vector dependent ($B = 0$) polarization given in Ref. 10, 11.

If one neglects the influence of the 2D relativistic electron gas the SAW propagation is a purely mechanical problem which is determined by the elastic constants. We don't make any specific assumptions about the bulk and top layer material but rather treat it as an isotropic piezoelectric medium characterized by longitudinal (L) and transverse (T) elastic constants or velocities c_β or $v_\beta = \sqrt{c_\beta/\rho}$ ($\beta = L, T$) respectively where ρ is the mass density. The stress-free boundary condition for the geometry in Fig. 1 is $\sigma_{iz} = 0$ ($i = x, y, z$). The solution of the boundary problem [17] leads to the velocity of the surface Rayleigh waves $v_s = \xi v_T$. Here v_s is smaller than the transverse bulk velocity by a factor $0.87 < \xi < 0.95$ depending on the ratio c_L/c_T . Due to the piezoelectric coupling an external potential is created which couples to the 2DEG via the density response function. The latter is completely determined by conservation laws and linear response relations. The induced density in the 2DEG leads to an additional energy density which has to be added to the elastic energy density causing a renormalization of the elastic constants or velocity. Because of the dissipative component in the density response the SAW velocity change is accompanied by an attenuation. It may be seen as Landau damping due to particle-hole excitations in the graphene sheet. By the above procedure [12] SAW velocity change Δv_s and attenuation coefficient κ are obtained as

$$\frac{\Delta v_s(q, B, \mu)}{v_s} - \frac{i\kappa(q, B, \mu)}{q} = \frac{\alpha(qd)^2/2}{1 + i\sigma_{xx}(q, \omega, B, \mu)/\sigma_m} \quad (2)$$

Here $\omega = v_s q$ is the SAW frequency and $\mathbf{q} \parallel x$ the wave number. The penetration depths $\kappa_L^{-1}, \kappa_T^{-1}$ of displacement components u_x, u_z into the bulk along $-z$ direction are of the order of the wavelength $\lambda = 2\pi/q$. The effective coupling $\alpha(qd)$ of SAW to the graphene 2DEG is a complicated expression composed of phenomenological parameters [12] which will not be given here. It depends nonmonotonically on qd and in the limit $qd \ll 1$ or $\kappa_{(L,T)}q \ll 1$ assumed here is simply a constant to be determined by experiment.

The central quantity is the longitudinal electronic conductivity $\sigma_{xx}(q, \omega; B, \mu)$ where $\omega = v_s q$. The normalization constant is $\sigma_m = v_s \epsilon_{eff}/2\pi$ with $\epsilon_{eff} = (\epsilon_0 + \epsilon)/2$ for $qd \ll 1$. The typical SAW frequency of ~ 0.1 GHz is extremely small ($\simeq 5 \times 10^{-3}$ K) compared to the typical electron hole excitation energy (given by the chemical potential μ so that one may use the static limit $\sigma_{xx}(q; B, \mu) = \sigma_{xx}(q, \omega = 0; B, \mu)$). We will consider two

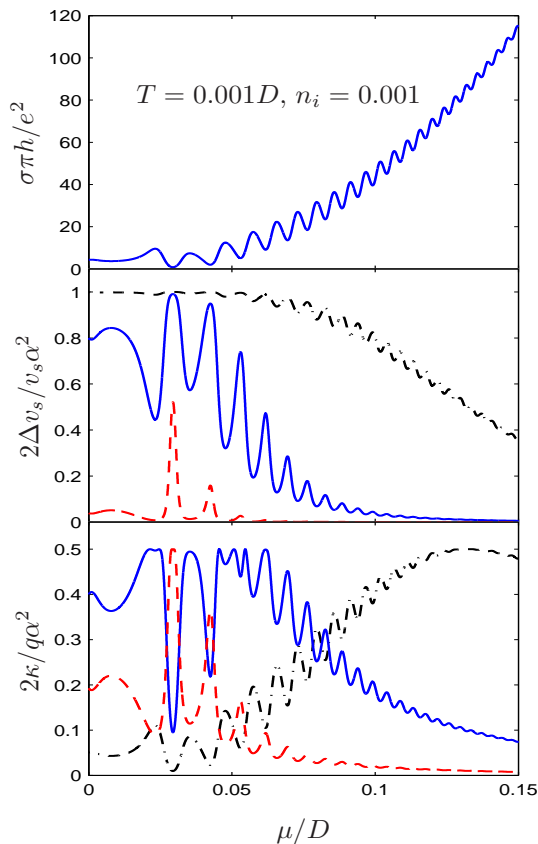


FIG. 2: Landau oscillations for constant field (corresponding to $N = 1000$ LL within the cutoff frequency D) as function of the chemical potential μ tuned by the gate voltage for $T = 0.001D$, $n_i = 0.001$. Upper panel: longitudinal conductivity. Middle/lower panel: SAW velocity change/attenuation for $\sigma_m/\sigma_{xx}(\mu = 0) = 10$ (black dashed-dotted line), 1 (blue solid line) and $1/10$ (red dashed line).

different cases: i) finite field case in the presence of scatterers, which allows to neglect the possible q dependence of the conductivity[18], if the scattering rate exceeds $v_F q$ and ii) zero field ultraclean case. For the former, due to Landau quantization, oscillations in $\Delta v_s(B, \mu)$ will appear both as function of field and as function of the chemical potential $\mu(V_g)$ or gate voltage V_g . The latter is an attractive new feature peculiar for SAW in graphene but not for the non-relativistic 2DEG. One may keep the field constant and instead observe the Landau oscillations as function of gate voltage. For the first case we need the field dependent conductivity $\sigma_{xx}(B, \mu)$ which was derived for localized disorder (vacancies representing the unitary limit[19]) in the self-consistent Born approximation (SCBA) in Ref. 16. The result is shown in the top panel of Fig. 2 as function of the chemical potential for a constant magnetic field for $\omega_c = D/\sqrt{N} + 1$ with $N = 1000$. Clearly the Landau oscillations in the conductivity also influence the SAW properties. When the chemical potential crosses a LL, the conductivity peaks, and Δv_s develops a dip. In between LL's, the conductiv-

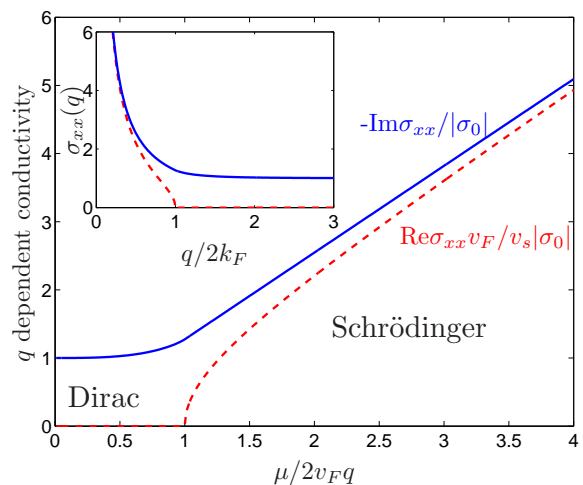


FIG. 3: Real (red dashed line) and imaginary (blue solid line) part of the conductivity for $B = 0$ as function of chemical potential and wave number (inset) with $|\sigma_0| = e^2 v_s / v_F$. The Dirac and Schrödinger like regions are separated at $2v_F q = \mu$.

ity is suppressed, causing the enhancement of the SAW velocity. For large chemical potential when the graphene sheet becomes more metallic, both Δv_s and κ are suppressed.

The SAW velocity measurement in zero field presents a unique feature which cannot be realized by the usual transport measurements, which usually probe the conductivity at $\omega \gg v_F q$, i.e. in the dynamic limit. Due to the finite SAW frequency the density response of the Dirac electrons may be probed at finite wave vector $q = \omega/v_s$ with $\omega \ll v_F q$, thus probing the static properties of the electric response. Measurement of Δv_s for various frequencies ω can therefore determine the density response of Dirac electrons for finite wave vector ω/v_s . This has actually been proposed and carried out for the non-relativistic 2DEG in Ref. 6.

The q ($\parallel x$) and ω dependent longitudinal conductivity is calculated similarly to the polarization function[10, 11], and is given in the limit of $\omega = v_s q \ll (\mu, v_F q)$ as

$$\sigma_{xx}(q) = \frac{4v_s e^2}{\pi v_F} \left[\frac{v_s}{v_F} f_1 \left(\frac{v_F q}{2\mu} \right) + i f_2 \left(\frac{v_F q}{2\mu} \right) \right], \quad (3)$$

where

$$f_1(x) = \frac{\sqrt{1-x^2}}{x} \Theta(1-x), \quad (4)$$

$$f_2(x) = -\frac{1}{x} + \frac{1}{2x} \left[\sqrt{1-\frac{1}{x^2}} - x \arccos \left(\frac{1}{x} \right) \right] \Theta(x-1), \quad (5)$$

and is shown in Fig. 3. It depends only on $v_F q/\mu$, thus exhibits scaling behaviour. For small frequencies, σ_{xx} vanishes with ω as follows from Eq. (6) via $\omega = v_s q$, which explains the v_s term on the r.h.s of Eq. (3). The

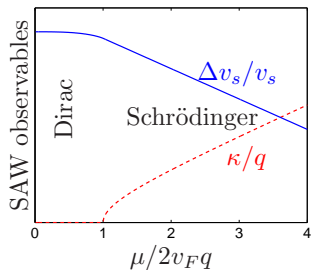


FIG. 4: Schematic view of the SAW velocity change (blue solid line) and attenuation (red dashed line) as a function of the chemical potential for $B = 0$ clean graphene. For small μ , the attenuation is negligible in the Dirac regime.

real part of the conductivity, which determines the attenuation, is suppressed by the additional v_s/v_F factor, thus the propagation velocity is more strongly influenced by the presence of graphene than the attenuation.

The density response or polarizability $\Pi(q)$ is related to the longitudinal conductivity by

$$\Pi(q_x, \omega) = \frac{iq_x^2}{\omega} \sigma_{xx}(q_x, \omega), \quad (6)$$

which follows from the charge continuity equation, and involves only the longitudinal component of the conductivity. For $\mathbf{q} = (q_x, 0)$, $q_x = q$. Using the equation for the SAW velocity change and neglecting the attenuation we may easily obtain

$$\Pi(q) \simeq q\sigma_m \left[\frac{\alpha^2}{2\Delta v_s(q)} - \frac{1}{v_s} \right] \quad (7)$$

from the measured velocity change. The density response for monolayer graphene has also been calculated in Ref. 10, 11, and SAW measurements can yield to the static polarizability as well.

There are two limits to be considered depending on whether q is larger or smaller than twice the radius of the Fermi circle $k_F = \mu/v_F$. For $2k_F > q$ what we refer to as Schrödinger like behaviour, $\sigma_{xx} = 8v_s e^2 k_F (\frac{v_s}{v_F} - i) / \pi v_F^2 q$, which holds true in a normal metal as well, and reveals the important k_F/q dependence of the conductivity. On the other hand, the peculiarity of graphene is the tunability of its Fermi energy with a gate voltage, which provides access to the $2k_F < q$ region, termed Dirac like regime, in which case $\sigma_0 = -ie^2 v_s/v_F$ exactly at the neutrality point ($\mu = 0$). Thus, there is practically no attenuation in this regime, only velocity renormalization. Typical SAW wavelengths range from 2-150 μm [20], which are translated to $v_F q \sim 2 - 200$ K using v_F for graphene. Graphene samples being ballistic over the micron-submicron scale imply a scattering rate around 50 K, thus, the above Dirac to Schrödinger like crossover can in principle be observed in clean samples with a tiny residual scattering rate at the neutrality point. The resulting behaviour of SAW observables are shown in Fig.

4, which resembles closely to that of the bare conductivity. We also speculate that SAW at $\mu = 0$ can identify the role inhomogeneities extending over several lattice constant (e.g. ripples, puddles) in graphene. When the SAW wavelength becomes comparable to their spatial extension, all waves passing through are scattered, and the sample is not transparent any more but acoustically opalescent.

In summary we have studied SAW propagation in monolayer graphene. By exploiting the chemical potential dependence of its conductivity, Landau oscillations are predicted in both the SAW velocity change and attenuation by varying the gate voltage, a feature which is only accessible due to the quasi-relativistic excitation spectrum in graphene, clearly absent in a normal 2DEG. SAW measurements in graphene can provide us with a deeper insight into the unconventional nature of the quantum Hall effect. Without magnetic field, the SAW frequency changes measure directly the wavevector dependence of the longitudinal conductivity, which can reveal a Dirac to Schrödinger like crossover, with no attenuation in the Dirac regime. In addition, SAW propagation in pristine graphene can yield significant information about the dominant scattering mechanisms close to the neutrality point through $\sigma_{xx}(q_x)$.

We are grateful to M. Polini, A. Hill and J. Ebbecke for useful correspondences. This work was supported by the Hungarian Scientific Research Funds under grant number K72613, and by the Bolyai program of the Hungarian Academy of Sciences

* Electronic address: dora@pks.mpg.de

- [1] R. Stoneley, Proc. Roy. Soc. **A232**, 447 (1955).
- [2] J. Heil, I. Kouroudis, B. Lüthi, and P. Thalmeier, J. Phys. C. **17**, 2433 (1984).
- [3] B. Lüthi, *Physical Acoustics in the Solid State* (Springer, Berlin, 2004).
- [4] A. Wixforth, J. P. Kotthaus, and G. Weimann, Phys. Rev. Lett. **56**, 2104 (1986).
- [5] R. L. Willett, M. A. Paalanen, R. R. Ruel, K. W. West, L. N. Pfeiffer, and D. J. Bishop, Phys. Rev. Lett. **65**, 112 (1990).
- [6] R. L. Willett, R. R. Ruel, M. A. Paalanen, K. W. West, and L. N. Pfeiffer, Phys. Rev. B **47**, 7344 (1993).
- [7] K. S. Novoselov, A. K. Geim, S. V. Morozov, D. Jiang, Y. Zhang, S. V. Dubonos, I. V. Grigorieva, and A. A. Firsov, Science **306**, 666 (2004).
- [8] A. K. Geim and K. S. Novoselov, Nature Materials **6**, 183 (2007).
- [9] A. H. Castro Neto, F. Guinea, N. M. R. Peres, K. S. Novoselov, and A. K. Geim, Rev. Mod. Phys. **81**, 109 (2009).
- [10] B. Wunsch, T. Stauber, F. Sols, and F. Guinea, New J. Phys. **8**, 318 (2006).
- [11] E. H. Hwang and S. D. Sarma, Phys. Rev. B **75**, 205418 (2007).

- [12] S. H. Simon, Phys. Rev. B **54**, 13878 (1996).
- [13] J. Fernández-Rossier, J. J. Palacios, and L. Brey, Phys. Rev. B **75**, 205441 (2007).
- [14] R. Arsat, M. Breedon, M. Shafiei, Spizziri, S. Gilje, R. B. Kaner, K. Kalantar-zadeh, and W. Wlodarski, Chem. Phys. Lett. **467**, 344 (2009).
- [15] M. Friedemann, K. Pierz, R. Stosch, and F. J. Ahlers, arXiv:0907.4080v1.
- [16] B. Dóra and P. Thalmeier, Phys. Rev. B **76**, 035402 (2007).
- [17] L. D. Landau and E. M. Lifshitz, *Theory of Elasticity* (Butterworth-Heinemann, Oxford, 2005).
- [18] R. L. Willett, Surf. Science **305**, 76 (1994).
- [19] N. M. R. Peres, F. Guinea, and A. H. Castro Neto, Phys. Rev. B **73**, 125411 (2006).
- [20] M. A. Paalanen, R. L. Willett, P. B. Littlewood, R. R. Ruel, K. W. West, L. N. Pfeiffer, and D. J. Bishop, Phys. Rev. B **45**, 11342 (1992).